Water at hydroxyapatite surfaces: the effect of coverage and surface termination as investigated by all-electron B3LYP-D* simulations

Water at hydroxyapatite surfaces: the effect of coverage and surface termination as investigated by all-electron B3LYP-D* simulations

Fabio Chiatti, Massimo Delle Piane, Piero Ugliengo & Marta Corno[†]

Dipartimento di Chimica, Università degli Studi di Torino and NIS – Nanostructured Interfaces and Surfaces – Centre, via P. Giuria 7, 10125 Torino, Italy

[†]Corresponding author. E-mail: marta.corno@unito.it

Abstract

Hydroxyapatite [HA, $Ca_{10}(PO_4)_6(OH)_2$], the main constituent of bones and teeth enamels, is a biomaterial commonly employed for prostheses and for repairing tissues. Previous theoretical and experimental studies have already characterized the physical-chemical basis of HA surfaces behavior towards water, ubiquitous molecule in biological fluids. Here, we extend such knowledge by simulating, at a hybrid DFT level of theory, different HA surface terminations, both stoichiometric and non-stoichiometric, as free and in interaction with water. This is done at an unprecedented accuracy, through the use of a large all-electron basis set and the inclusion of dispersion forces contributions. The calculated results are then compared with experimental microcalorimetric data, showing a good agreement in the loading trend of the (010) surfaces. More generally, this theoretical approach is confirmed to be an efficient tool to analyze these materials, giving the possibility to investigate the HA behavior towards more complex molecules, from aminoacids to collagen, at the here presented level of theory.

Introduction

Biomaterials are a class of compounds, which elicit an appropriate response when interacting with biologically active molecules (drugs, amino acids, etc…).REF Within this field, hydroxyapatite ($Ca_{10}(PO_4)_6(OH)_2$, HA) has soon become subject of detailed studies because it constitutes the mineral phase of bones and teeth. Clearly, HA in the bone structure is not crystalline nor un-substituted, as many punctual defects, either cationic such as Mg^{2+} and Na^{+}, or anionic such as F^{-} and CO_3^{2-}, are present. Moreover, the bone structure is not only composed by a mineral phase but has also an organic matrix, mostly composed by collagen and other polypeptides.REF How these molecules interact with the mineral substrate is still an open question, together with the possibility of changing or varying some interfacial properties. Along this line, some of us have recently published a study of the dipolar behavior of the (001) surface of HA, in which a hypothesis based on the dipole-dipole interaction has been advanced.[1]

Beyond all these considerations, the hydroxyapatite material, even if crystalline or synthesized, is widely accepted to be one of the most biocompatible substrate which can be successfully exploited for building prostheses, for repairing micro-fractures in tissues, even as a component of toothpastes for preventing teeth slicing.ref Therefore, studies on HA structure have rapidly become very important, aiming at the understanding of its large bio-response at a molecular level.

In this paper, we intend to investigate the role of water, as omnipresent in biological fluids, when interacting with the different surfaces of hydroxyapatite. Some of us, in previous articles, have already described the two most important HA surfaces, i.e. the (001) and the (010), alone and in interaction with water and other biomolecules,REF but the level of theory was lower than the current paper (pseudopotential for the description of calcium core electrons and a double-ζ for all the other elements). Moreover, in 2008, a paper by Astala and Stott introduced the models of two new (010) non-stoichiometric surfaces, which may represent other terminations of the material along this direction.[2] This possibility has already been confirmed by experimental HR-TEM study, ref which highlighted the existence of different terminating layers along the [010] direction. Nonetheless, a description at a molecular level of the surfaces was still needed and the level of computational accuracy was limited to a numerical basis set (SIESTA code), with the PBE functional.

The purpose of this article is a full description of geometrical and electronic properties of the most relevant HA surfaces, reviewing and updating what has already been done by us, but also introducing the (010) non-stoichiometric surfaces and other two stoichiometric ones, the (101) and the (110). All the surfaces are, then, studied either alone or interacting with water. The CRYSTAL code has been adopted, in its 2014 release, increasing the level of theory to the B3LYP hybrid

functional, employing double-ζ and triple-ζ all-electron basis sets of proved quality.

Computational details

All the presented structures were simulated with the *ab initio* periodic CRYSTAL14 code.[3] The Kohn-Sham[4, 5] Hamiltonian is implemented in CRYSTAL14, for the study of chemical systems of any periodicity (from molecules to crystals). MOLDRAW,[6] QUTEMOL[7] and VMD[8] were employed for manipulating and visualizing the structures and the isodensity maps.

Basis set

The multi-electron wave function was described by linear combination of crystalline orbitals, which, in turn, were expanded in terms of Gaussian-type basis set functions. In the present work, the Ca atoms were described with a triple-ζ valence all-electron basis set, 86-811G(3d), with α_{sp} = 0.295 bohr^{-2} as the exponent of the most diffuse shell and α_{pol} = 0.3191 bohr^{-2} for polarization. A 85-21G(d) basis set was used for P atoms, with α_{sp} = 0.1350 bohr^{-2} as the most diffuse shell exponent and α_{pol} = 0.7458 bohr^{-2} for polarization. O atoms were represented with a 511111-411G(d) basis set (Ahlrichs VTZ), with α_{sp} = 0.1751 bohr^{-2} as the most diffuse shell exponent and α_{pol} = 0.1200 bohr^{-2} for polarization.[9] H atom was described by 31G(p) basis set, with α_{sp} = 0.1613 bohr^{-2} as the most diffuse shell exponent and α_{pol} = 1.100 bohr^{-2} for polarization.[6]

Hamiltonian, geometry optimization and vibrational frequencies calculation

All simulations were performed within the Density Functional Theory (DFT) framework employing one of the most diffuse hybrid functional, the B3LYP.[10, 11] This functional had already been adopted by our group, providing results in good agreement with the experimental data.[12–15]

The DFT exchange-correlation contribution was calculated with a numerical integration of the electronic density over a pruned grid of 75 radial points, with one sub-interval of 974 angular points. The Hamiltonian matrix was diagonalized over 4 *k*-points.[16] The tolerances controlling the accuracy of the Coulomb and exchange series needed to build up the Fock matrix were set to 10^{-6}, whereas the pseudo-overlap truncation criteria for the Hartree-Fock exact exchange was set to 10^{-14}.[17]

Internal coordinate optimization was performed *via* an analytical gradient method, upgrading the numerical Hessian with the Broyden-Fletcher-Goldfarb-Shanno algorithm.[18, 19] The remaining parameters, such as the integrated density, the maximum and the RMS of gradient component, the maximum and the RMS of the displacement component, were kept as their default values (respectively, 10^{-6} electrons, $4.5\cdot10^{-4}$ hartree·bohr^{-1}, $3\cdot10^{-4}$ hartree·bohr^{-1}, $1.8\cdot10^{-3}$ bohr, $1.2\cdot10^{-3}$

bohr).

Interaction Energy and Enthalpy of Adsorption

In the periodic treatment of surface adsorption processes, the interaction energy (ΔE) per water molecule per unit cell is defined as the net averaged energy required to remove the *N* adsorbate molecules (here water) from the surface to the gas phase, according to the following expression:

$$\Delta E = \frac{1}{N}[E(SW // SW) - E(S // S) - N \cdot E_M(W // W)] \quad (1)$$

where E(S//S) is the energy of the bare slab S in its optimized geometry, E_M(W//W) is the molecular energy of the free water molecule in its optimized geometry, and E(SW//SW) is the energy of the surface/adsorbate system in its optimized geometry (the symbol following the double slash, //, identifies the geometry at which the energy is computed). Therefore, ΔE is a negative quantity for a bound adsorbate.

The deformation energies due to the adsorption process of both the surface and the adsorbate are reported in Equations (2) and (3), respectively. δE_S represents the deformation energy of the surface per adsorbed molecule, i.e. it is the averaged difference between the energy of the slab in the optimized geometry of the surface/adsorbate system and the energy of the free slab. The deformation of the molecule δE_W can be divided into two quantities: the first one, ΔE_W of equation (4), depends on the geometrical changes (variation in interatomic distances, angles, etc…) and is defined as the averaged energy required to deform one molecule from the optimized geometry to that of the surface/adsorbate system; the second one, ΔE_L, reported in Equation (5), corresponds to the lateral interactions among the adsorbed molecules and is defined as the averaged difference between the energy of the layer of the N adsorbed molecules and the sum of the energies of each deformed molecule.

All contributions are averaged on the total number of molecules N:

$$\delta E_S = \frac{1}{N}[E(S // SW) - E(S // S)] \quad (2)$$

$$\delta E_W = \frac{1}{N}[E(\sum_{i=1}^{N} W_i // SW) - N \cdot E_W(W // W)] = \Delta E_W + \Delta E_L \quad (3)$$

$$\Delta E_W = \frac{1}{N}\left[\sum_{i=1}^{N} E_W(W_i // SW) - N \cdot E_w(W // W)\right] \quad (4)$$

$$\Delta E_L = \frac{1}{N}[E(\sum_{i=1}^{N} W_i // SW) - \sum_{i=1}^{N} E_W(W_i // SW)] \quad (5)$$

The deformation contributions, δE_S and ΔE_W are always positive, as both the molecules and the slab

change their geometry from that of the minimum energy structure, because of the adsorption process. On the contrary, the lateral interactions ΔE_L can be either positive (repulsive) or negative (attractive). This term is affected by two problems. The first concerns the basis set superposition error (BSSE): when dealing with a localized basis set, the energetic differences, whose terms are calculated with different numbers of basis functions, have to be corrected for this error. For the lateral interactions, the BSSE correction becomes important when more than one molecule is adsorbed in the same unit cell. We applied the widely accepted counter-poise method, proposed by Boys and Bernardi,[20] to estimate and correct this error for ΔE_L, through addition of ghost functions:

$$\Delta E_L^{\ C} = \frac{1}{N}[E(\sum_{i=1}^{N} W_i \,//\, SW) - \sum_{i=1}^{N} E(W_i \sum_{j\neq 1}^{N} [W_j] // SW)] \qquad (6)$$

$E(W_i \sum_{j\neq 1}^{N} [W_j] // SW)$ is the energy of a slab in which the i-th molecule, in the adduct geometry, is real while all the other molecules in the j-th sum are ghosted. In this way, we only neglect the BSSE due to the periodic images of the same molecule, which is, indeed, negligible if the slab unit cell is large enough.

The second term affecting the lateral interactions ΔE_L is the presence of dispersive contributions, which should be taken into account by defining the ΔE_L, as in Eqaution

With these positions, it is possible to define a binding energy free of deformation and lateral interactions terms, which considers only the quantistic interaction energy between a layer of deformed water molecules and a deformed HA surface, as reported in Equation 5:

$$BE^* = BE + \Delta E_S + \Delta E_M + \Delta E_L = \frac{1}{N}[E(S \,//\, SW) + E(\sum_i W_i \,//\, SW) - E(SW \,//\, SW) \qquad (5)$$

When dealing with a localized basis set, the energetic differences, whose terms are calculated with different numbers of basis functions, have to be corrected for the basis set superposition error (BSSE). Hence, BE, BE* and ΔE_L are affected by this error and have to be corrected. We applied the widely accepted counter-poise method to estimate and correct this error for BE* and ΔE_L, through addition of ghost functions.(ref) The BSSE correction to the ΔE_L term is important when dealing with more than one water molecule adsorbed in the same unit cell.

$$BE^{*C} = \frac{1}{N}[E(S\sum_i [W_i] // SW) + E([S]\sum_i W_i \,//\, SW) - E(SW \,//\, SW)] \qquad (6)$$

$$\Delta E_L^C = \frac{1}{N}[E(\sum_i W_i \,//\, SW) - \sum_i E(W_i \sum_{j\neq i} [W_i] // SW)] \qquad (7)$$

$E(S\sum_i [W_i] // SW)$ and $E([S]\sum_i W_i \,//\, SW)$ are the total energy of the HA slab with the ghost

functions of the water layer and vice-versa. $E(W_i \sum_{j \neq i}[W_j] // SW)$ is the energy of the *i*-th molecule, in the adduct geometry, with all the other molecules ghosted.

The BE is, then, corrected indirectly from the corrected terms:

$$BE^C = CE^{*C} - \Delta E_S - \Delta E_M - \Delta E_L^C \quad (8)$$

The BSSE is, thus, calculated as:

$$BSSE = BE - BE^C \quad (9)$$

The same treatment discussed here has already been used by some of us for the study of the interaction between glycine and water with silica and hydroxyapatite surfaces.(ref)

It is widely known that DFT cannot properly take into account the dispersive forces. We adopted the Grimme's correction, properly rescaled for the B3LYP functional, to estimate the dispersion contribution. Hence, we defined a BE, only due to the dispersion, as:

$$BE^D = \frac{1}{N}[E^D(S // S) + N \cdot E_M^D(W // W) - E^D(SW // SW)] \quad (10)$$

The sum of BE^C and BE^D is still an electronic energy, thus not comparable to the heat of adsorption, as the thermal effects are not accounted for yet. According to the statistical thermodynamics, the enthalpy values at a T temperature are defined as:

$$\Delta H(T) = -BE^C - BE^D + \Delta ZPE + \Delta E_T \quad (11)$$

As we only considered the vibrational frequencies of the adsorbed molecules, the ΔZPE is defined as the averaged difference between the zero-point energy of the adsorbed molecules in the adduct system and the zero-point energy of the free molecule (Equation 12). This derives from the shifts of the 3N-6 vibrational frequencies of the gas phase to the 3N vibrations in the adduct system. Indeed, the 6 rotations and translations of the molecule fall at 0 cm^{-1} for the gas phase but become non-null when the molecule interacts with a substrate. On the contrary, the ΔE_T considers 3 rotational, 3 translational and 3N-6 vibrational contributions to the total enthalpy for the gas phase. 3N vibrational contributions are, instead, considered for the adsorbed molecule in the adduct system.

$$\Delta ZPE = \frac{1}{2}h\sum_i \Delta \nu_i = \frac{1}{N}[ZPE(N \cdot W // SW) - N \cdot ZPE_M(W // W)] \quad (12)$$

$$\Delta E_T = \frac{1}{N}[E_T(N \cdot W // SW) - N \cdot \Delta E_{T\,M}(W // W)] \quad (13)$$

Electronic Features of the HA Surfaces

We have characterized the electronic features of the HA surfaces by computing : i) the surface energy; ii) the band gap; iii) the value of the dipole moment across the slab; iv) the electrostatic

potential mapped onto an isodensity surface. The latter three properties are directly calculated by the CRYSTAL code while the first one is more complex.

Within the slab model approach, the surface energy for stoichiometric surfaces is computed as follows:

$$E_{surf} = \frac{E_{slab} - 2 \cdot E_{bulk}}{2A} \quad (14)$$

Where E_{slab} is the energy of a double layer slab, E_{bulk} is the energy of a (monolayer) unit cell of HA bulk and A is the area of the slab cell (doubled because two faces are exposed). According to this equation, the two faces are considered equivalent. For the (001) and (101) surfaces, which do not have a centro-symmetric orientation of the OH^- column, the surface energy yields to the average between the two faces. This is not problematic and is fully justified by a previous work by some of us, which highlighted that the surface energy of the (001) surface is not affected by the dipole moment of the OH^- column.(ref)

As non-stoichiometric surfaces have a fractional number of layers (between 2 and 3, in our models) with respect to the bulk unit cell, the surface energy cannot be defined using Equation 14. According to what Astala and Stott did,[17] we estimated the surface energy of the non-stoichiometric surfaces by considering appropriate reference systems. More details will be reported in the results and discussion part.

Results and discussion

This section is divided into two paragraphs, the first one describing the HA structures and the second one reporting the results of the adsorption of water upon the HA surfaces.

HA bulk and surfaces

The bulk structure

Hydroxyapatite is a mineral, which occurs in nature in two polymorphs, the monoclinic form (*$P2_1/b$*), thermodynamically stable at low temperatures, and the hexagonal form (*$P6_3/m$*), naturally present in the bone structure, which can be easily stabilized by substitution of the OH^- ions.

The crystallographic difference between the two polymorphs relies upon the orientation of the OH^- ions, which are found in columns along the *c* axis. The monoclinic unit cell, shows two columns, which point in the two opposite directions ([001] and [00$\bar{1}$]). Conversely, the hexagonal form is characterized by one column only, which is compatible with the crystallographic mirror plane because of the intrinsic static disorder of these ions, highlighted by fractional occupation factors

(50% probability for each direction). As *ab initio* simulation cannot take into account the structural disorder, we reduced the symmetry to $P6_3$, removing the mirror plane and fixing the directions of the OH^- ions. In the most stable configuration, all the OH^- ions point in the same direction. In the present paper, we refer only to this bulk structure and all the slab structures are derived from this hexagonal polymorph. This bulk structure has already been fully characterized in literature by some of us in the past, employing the B3LYP functional and a basis set of double-ζ with polarization quality (DZP) and an effective core pseudopotential (ECP) for the 10 core electrons of calcium atoms.(ref PCCP) This structure has been considered the starting geometry and has been optimized with the current computational parameters (section B). After the optimization, the lattice constants of the hexagonal cell have resulted: a = b = 9.635 Å; c = 6.854 Å; α = β = 90.0°; γ = 120.0° (the angles are fixed by the symmetry of the space group). These results are in better agreement with the experimental values obtained through neutron diffraction at 298 K (a = b = 9.425 Å; c = 6.884 Å), (ref Saenger & Kuhs) than those computed with a DZP – ECP basis set (a = b = 9.329 Å; c = 6.949 Å).(ref)

From this structure, we modeled the surfaces which are experimentally found to be the most important: (001) and (010), the latter identical by symmetry to the (100). These surfaces have already been fully characterized at the B3LYP level by some of us and were also studied in adsorption with different typologies of molecules, that span from water to organic acids, amino-acids and small peptides, providing results comparable with the experimental heats of adsorption. In the present paper, these surfaces have been modeled again, keeping the cell parameters fixed at those obtained from the current bulk optimization.

In the present paper, we also model, for the first time at the B3LYP level, the (101), identical to the (011), and the (110) surfaces. The first one has already been studied with a pure GGA functional,(ref Wierzbicki & Cheung) highlighting the presence of the (101) surface in the crystalline habit of HA. The (110) surface is, instead, modeled for the first time.

The (001) surface

The (001) surface is generated by cutting the bulk structure along the plane defined by the *a* and *b* vectors (hence, perpendicularly to the *c* axis). There is only one possibility to terminate the surface, as all the layers are equivalent and keep the composition of the whole structure.

The (001) surface, as cut from the $P6_3$ bulk in which the OH- ions are ordered (vide supra), shows a column of OH^- ions which generate a dipole moment across the slab. The ferroelectric features of the (001) surface have recently been studied by some of us.(ref JPCC) We have computed geometries, surface energies and electronic feature of slab models of variable thickness, up to a 43

nm, showing that the ferroelectric OH^- alignment does not compromise the stability of the HA (001) surface at a nanometric scale. No sign of instability occurred, differently from classical polar surfaces, because of the counter-polarization acted by Ca^{2+} and PO_4^{3-} moieties surrounding the OH^- arrays. The (001) surface superimposed to the isodensity surface colorcoded with the electrostatic potential is reported in Figure 1.

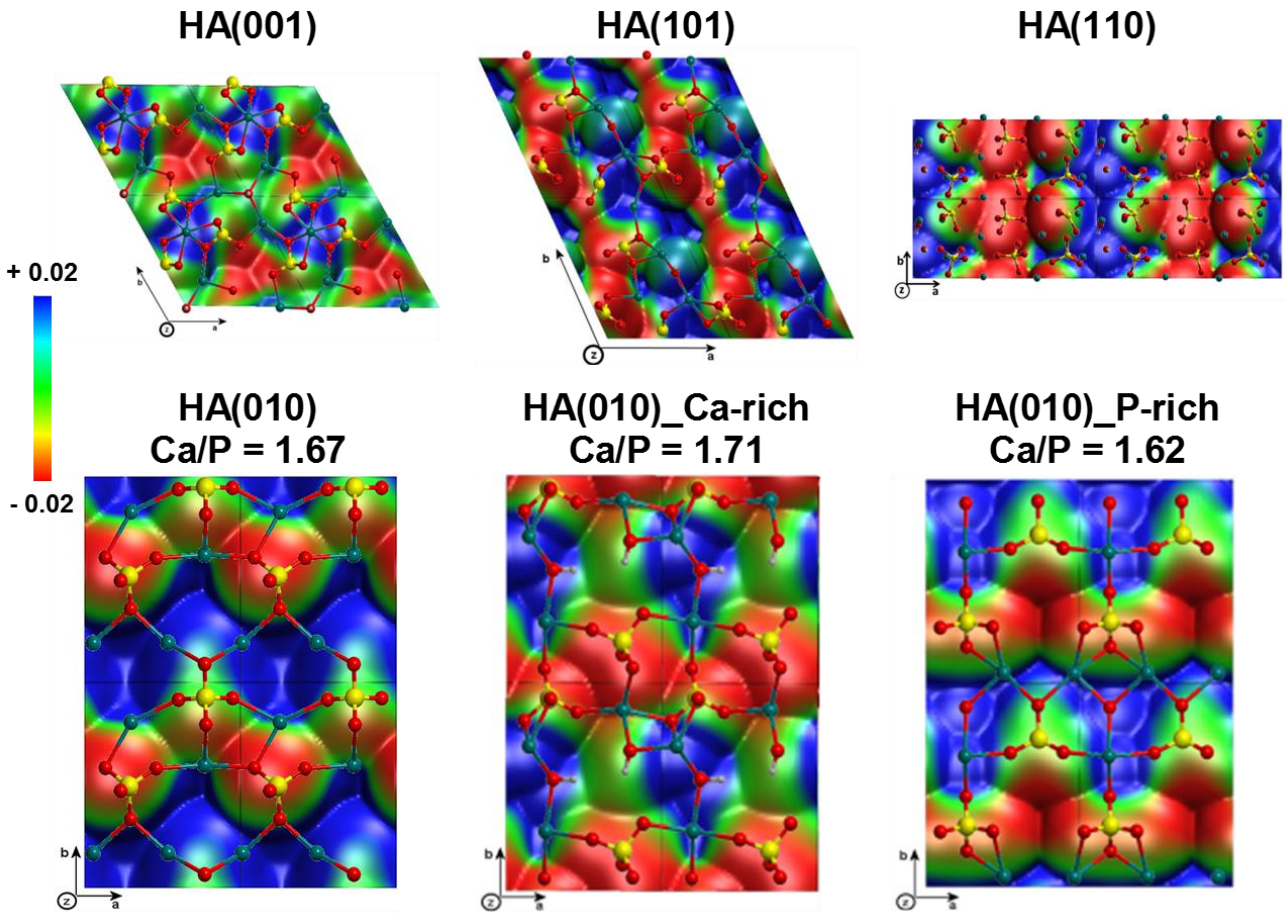

Figure 1. Studied HA surfaces, superimposed to the isodensity surface colorcoded with the electrostatic potential. $\rho = 10^{-6}$ a.u., V from -0.02 a.u. (red) to 0.00 a.u. (green) to +0.02 a.u. (blue). Color-coding for the atoms: oxygen in red, hydrogen in white, calcium in blue/green, phosphorus in yellow.

The potential is completely influenced by the most exposed ions of the surface: the positive zone is located close to the most exposed calcium ion while the negative region is originated by three phosphate ions. The OH^- ions do not generate a strong potential, as highlighted by the green color of the map. The surface energy calculated with equation 14 is 0.047 $eV \cdot Å^{-2}$, lower than the value found by other groups.(ref)

The (010) surfaces

The (010) surface is generated by cutting the periodic bulk structure along the plane defined by the

cell axes *a* and *c* (or, alternatively, *b* and *c*). The OH^- ions column lays, thus, parallel to the face and do not generate any dipole moment across the slab structure. This surface is not uniquely defined, as highlighted by HRTEM studies.(ref) Indeed, there are two kinds of layers with different composition: $Ca_3(PO_4)_2$ (A-type) and $Ca_4(PO_4)_2(OH)_2$ (B-type). As the sequence is …-A-A-B-A-A-B-A-A-B-…, the periodicity can be interrupted in three ways, exposing as last layers: i) …-A-B-A or ii) …-A-A-B or iii) …-B-A-A. In order to avoid geometrical dissimilarities, which could prevent the stability of the structure, the most exposed layers, on top and bottom faces of the slab, ought to be similar, to remove any possible dipole moment across the slab. This necessity brings the loss of stoichiometricity in two cases: as a matter of fact, neither B-A-A-B-A-A-B nor A-A-B-A-A-B-A-A can be replicated to regenerate the bulk. Only the sequence A-B-A-A-B-A preserves this possibility, with a Ca/P ratio of 1.67. Our group has already studied the (010) stoichiometric surface many times, alone and in interaction with several classes of compounds.(ref) As the B layers are not exposed, the hydroxyl ions are not present on top of the slab structure and the color-coding of the isodensity surface is uniquely due to calcium and phosphate ions (Figure 1). A very extend blue clump in the middle of this surface shows its large reactivity towards polar molecules: indeed, this termination can easily deprotonate adsorbed molecules (water, carboxyl acids, aminoacids, etc…). The larger reactivity of this surface is not an artifact of the functional, as it has been confirmed many other times either by our group or by independent studies of other groups.(ref) The large reactivity brings the surface to generate new superficial CaOH and POH moieties. This is wider described in the 3.2.1 paragraph. The surface energy for the stoichiometric (010) surface, calculated with equation 14, is 0.084 $eV \cdot Å^{-2}$.

Recently, some of us also published some preliminary results concerning the analysis of the two (010) non-stoichiometric surfaces but, here, the discussion is much more detailed. When the most exposed layers are –B-A-A, the surface is called P-rich because the Ca/P ratio decreases to 1.62 (Figure 1). The (010) slab structure terminating in –A-A-B is called Ca-rich, with an increase of the Ca/P ratio to 1.71 (Figure 1). As the most exposed layer is B-type for the (010) Ca-rich surface, the OH^- ions are exposed on top of the slab. Nonetheless, as already found for the (001) surface, they do not influence the electrostatics, resulting completely plunged in the potential generated by the most exposed calcium ions. Due to the non-stoichiometric nature, the surface energy of these structures cannot be defined using equation 14 but needs some reference systems, as explained below.

The energy of the P-rich surface (A-A-B-A-A-B-A-A) is not commensurable to twice that of the bulk structure (twice -A-B-A-), because of two A layers which are present in the slab definition and missing in the bulk. Analogously, the energy of the Ca-rich surface (B-A-A-B-A-A-B), because of

one additional B layer in the slab structure. In order to simplify the problem for the Ca-rich surface, it is easier to consider the comparison between the energy of the Ca-rich structure and three times that of the bulk. Of course, the two energies are still incommensurable, because of two A layers present in the bulk and missing in the slab, but, at least, both the non-stoichiometric surface energies depend only on the A layer. Indeed, it is possible to calculate the surface energies with these equations:

$$E_{surf,P-rich} = \frac{E_{slab,P-rich} - 2E_{bulk,HA} - 2\mu_A}{2A} \quad (15)$$

$$E_{surf,Ca-rich} = \frac{E_{slab,Ca-rich} - 3E_{bulk,HA} + 2\mu_A}{2A} \quad (16)$$

Where μ_A is the chemical potential of the A layer. In order to calculate μ_A, we considered two reference systems:

ii) considering the reaction of decomposition of HA in $Ca_3(PO_4)_2$ and the most stable polymorph of $Ca(OH)_2$, portlandite (CH):

$$Ca_{10}(PO_4)_6(OH)_2 \rightarrow Ca(OH)_2 + 3\ Ca_3(PO_4)_2 \quad (18)$$

$$\mu_1 = \frac{1}{3}[E_{HA} - E_{CH}] \quad (19)$$

where E_{HA} and E_{CH} are the electronic energies, per formula unit, calculated for the optimized hexagonal ($P6_3$) hydroxyapatite and the optimized trigonal ($P\bar{3}m1$) portlandite bulk structures.

i) the most stable polymorph of $Ca_3(PO_4)_2$, the β-tricalcium phosphate (β-TCP),

$$\mu_2 = E_{\beta-TCP} \quad (17)$$

Where $E_{\beta\text{-}TCP}$ is the electronic energy, per formula unit, calculated for the optimized trigonal ($R3$) bulk β-TCP;

Thermodynamically, it is found that $\mu_1 < \mu_2$, meaning that $E_{HA} < E_{CH} + 3 \cdot E_{\beta-TCP}$, i.e. that HA is more stable than the most stable phases of the reactants (CH and β-TCP). It is also clear that the stability region of the HA non-stoichiometric surfaces, which depends on μ_A, is between these two limit situations: indeed, if $\mu_A > \mu_2$, calcium phosphate precipitates as β-TCP and is no more available for the surfaces. On the other hand, if $\mu_A < \mu_1$, this signifies $E_{HA} > E_{CH} + 3 \cdot \mu_A$ and HA would decompose. These constraints lead to the stability window also identified by Astala and Stott: $\mu_1 \leq \mu_A \leq \mu_2$.

The results of the surface energies for P-rich and Ca-rich (010) surfaces are, respectively, 0.070 eV·Å^{-2} and 0.062 eV·Å^{-2} when $\mu_A = \mu_1$ and 0.062 eV·Å^{-2} and 0.071 eV·Å^{-2}, when $\mu_A = \mu_2$.

Equations 15 and 16 highlight the linear trend of the surface energies with respect to μ_A, hence it is

possible to plot the surface energies, linearly interpolating the two boundary points.

The (101) surface

The (101) surface was firstly considered by Wierzbiki & Cheung as the second most important, in terms of extent in the crystalline habit, but they did not provide any geometrical description of the surface. In principle, this surface should present the OH^- channel crossing diagonally the slab structure, as the cut from the bulk takes place along the diagonal of the rectangle defined by the *a* and the *c* axes (or, eventually, the *b* and *c* axes). This surface do not generate non-stoichiometric surfaces, as all the layers of the slab have the same composition of the bulk (as well as the (001) surface), thus only a stoichiometric surface can be modeled. When the optimization is performed, a strong relaxation involves the most exposed OH^- ions on both sides, which rotate and become oriented almost perpendicular to the slab cell vectors. Conversely, the internal ions do not suffer any relevant displacement and do not lose the diagonal orientation. The rotation of the outermost ions has already been observed by Astala and Stott who also recognized, but did not quantify, a dipole moment across the (101) slab. Anyway, except for the internal OH^- ions which remain aligned, the two faces are very similar, hence we report only the topmost face (Figure 1). Rows of positive and negative potential can be seen, in correspondence of the outermost calcium and phosphate ions. The surface energy is 0.066 $eV \cdot Å^{-2}$.

The (110) surface

The (110) surface was only hypothesized by Rulis et al. (Phys Rev B, 2007, 76, 245410) but no one has modeled it yet. This surface is generated cutting the bulk along the major diagonal of the parallelogram plane defined by the *a* and *b* axes. Because of this geometrical definition, the cell area is larger than the previous slab structures and causes a smaller thickness of the slab. The small thickness (8.6 Å) allows large displacements during the relaxation of the structures. Indeed, the OH^- ions, which should not be exposed, are able to find a pathway through the other atoms and rumple, approaching to the most exposed calcium ions. Nonetheless, they do not modify the electrostatic potential, as highlighted in Figure 1. The surface energy is 0.076 $eV \cdot Å^{-2}$.

Comparison between the HA surfaces and Wulff construction

In Table 1, a geometrical analysis of the bulk and slab structures is reported. The Mulliken charges do not vary with the system and confirm the ionic nature of HA, even if the total charges are not very close to those assigned to the free ions. Also the interatomic distances and angles are very similar among the structures. It is noteworthy the increase of the standard deviations of the

geometrical parameters, when moving from the bulk to the slab structures. This is partially due to the loss of symmetry, because all the surfaces have less or even no symmetry elements; the most important reason is the loss of the crystalline field periodicity along the third dimension. Indeed, the lack of translational symmetry implies that the equilibrium of the forces for the bulk is not maintained in the slab system, as many forces are no more present. Consequent rearrangements modify the structure and cause the dispersion of distances and angles around their midpoints, which are instead mostly preserved.

Table 1. Main features of HA bulk and surfaces: net Mulliken charges of Ca^{2+}, PO_4^{3-} and OH^- ions (*e*), averaged interatomic distances Ca-O, P-O and O-H with the correspondent standard deviations (Å), averaged OPO angle with the correspondent standard deviation (°), electronic Band Gap (BG/*eV*) and Dipole Moment across the slab (D/*Debye*), Thickness (T/*Å*) computed as the perpendicular distance between the most exposed Ca^{2+} ions on the top and bottom faces , number of exposed Ca^{2+} ion *per* surface unit cell (Ca/S).

HA System	Ca^{2+}	PO_4^{3-}	OH^-	<Ca-O>	<P-O>	<O-H>	<O$\hat{P}$O>	BG	D	T	Ca/S
Bulk	1.79	-2.69	-0.87	2.43±0.05	1.55±0.01	0.97±0.00	108.1±1.8	7.51	---	---	---
(001)	1.78	-2.67	-0.86	2.42±0.07	1.55±0.01	0.97±0.00	108.2±2.7	7.54	0.38	13.1	4
(010) Stoich	1.77	-2.67	-0.86	2.41±0.07	1.55±0.03	0.97±0.00	108.8±3.5	6.17	0.07	13.3	4
(010) Ca-rich	1.77	-2.67	-0.85	2.40±0.07	1.55±0.05	0.97±0.00	110.3±5.1	6.64	0.00	20.1	3
(010) P-rich	1.77	-2.66	-0.86	2.40±0.08	1.55±0.02	0.97±0.00	109.4±2.9	6.51	0.00	20.2	3
(101)	1.77	-2.66	-0.85	2.40±0.07	1.55±0.02	0.97±0.00	109.5±4.3	7.15	0.01	10.3	4
(110)	1.76	-2.64	-0.86	2.41±0.15	1.55±0.03	0.97±0.00	109.2±5.3	6.37	0.92	8.6	4

Two important intensive parameters can classify the stability of a slab structure: the electronic band gap and the total dipole moment across the slab. Among the slab, the (001) surface presents the largest band gap and a rather small dipole moment. These features have been widely described in details by some of us recently.(ref) All the three (010) surfaces have a negligible dipole moment and the band gap slightly smaller than the (001), but still in the range of insulator systems. Unexpectedly, the (101) surface presents a small dipole moment, meaning that the described rearrangement of the OH^- ions annihilates the intrinsic dipolarity of the ferroelectric diagonal alignment of the OH^- ions. Conversely, the (110) surface, which should not be dipolar as the OH^- ions lay parallel to the face, presents a quite large dipole moment, almost 1 Debye. This dipole moment takes origin from the very large displacements of the atoms, which generate geometrical dissimilarities between the two faces after the optimization procedure. The band gap remains, anyway, rather high.

The slab thickness is always larger than 10Å, except for the (110) surface, ensuring a good

representation of the surface at a controlled computational cost. The thicknesses of the (010) non-stoichiometric surfaces are the largest ones, because of additional A and B layers, requested to avoid the dissimilarities among the faces (*vide supra*).

In order to compare the surface energies, we plotted the surface energies as functions of the chemical potential $Ca_3(PO_4)_2$ (Figure 2).

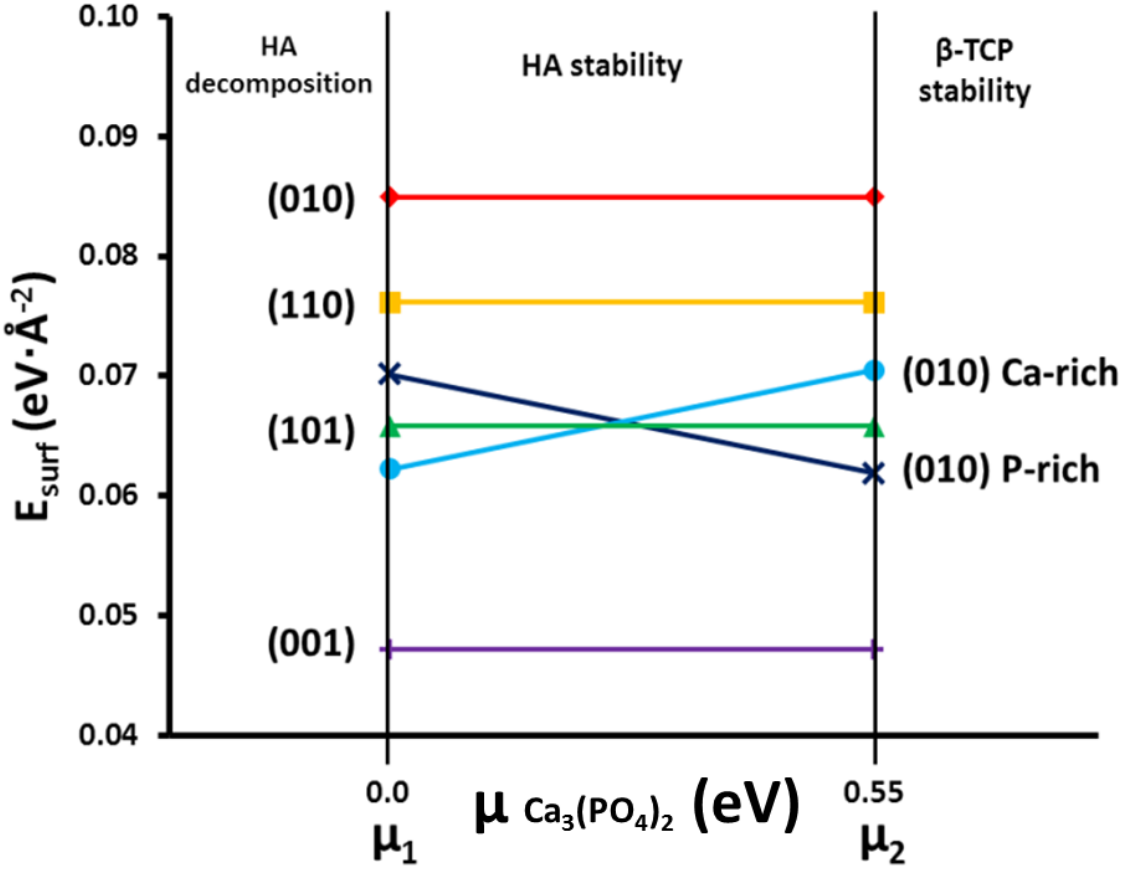

Figure 2. Surface energies (E_{surf}/eV·Å^{-2}) of the studied HA surfaces as functions of the chemical potential of calcium phosphate (μ_A/eV). The stability window of HA is reported in the upper captions.

For the sake of clarity, we fixed at 0 eV the chemical potential of μ_2. Consequently, μ_1 has been calculated to be 0.55 eV. All the stoichiometric surface energies do not depend on the chemical potential of calcium phosphate (μ_A), resulting horizontal lines (Equation 14). Conversely, the non-stoichiometric surface energies vary linearly with the chemical potential, according to Equations 15 and 16. The (001) surface is found to be the most stable surface, in agreement with what found by several other authors.(ref) In agreement with previous theoretical and HRTEM experimental results,(ref) the stoichiometric (010) surface is not the most stable termination along the [010] direction, with a much higher surface energy with respect to the non-stoichiometric systems. The relative stability among the non-stoichiometric surfaces changes with the chemical potential of $Ca_3(PO_4)_2$, as the two curves cross one another. Differently from the published plot by Astala and

Stott, we found that the curves representing the non-stoichiometric surface energies have an opposite slope as, according to equations 15 and 16, the Ca-rich surface energy increases with the chemical potential μ_A, and vice-versa for the P-rich. Moreover, the cross we found falls inside the stability window defined by HA, CH and β-TCP. From the surface energy results, we calculated the Wulff construction, reproducing the crystalline habit of HA: the distance of each family plane from the center of the structure is inversely proportional to the correspondent surface energy. Hence, the smaller the surface energy, the smaller the distance from the center and the larger the exposure on the crystalline habit (Figure 3).

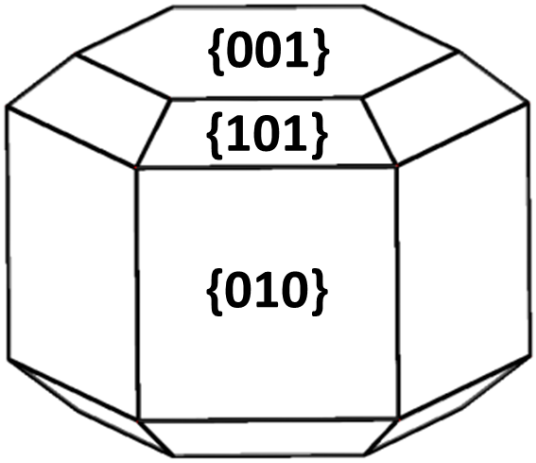

Figure 3. Wulff construction reproducing the crystalline habit of HA.

We selected the value of 0.062 eV·Å^{-2} as surface energy of the {010} family, as it the lowest value for a (010) surface energy (assumed by the (010) Ca-rich surface at $\mu_A = \mu_1$ and by the (010) P-rich surface at $\mu_A = \mu_2$).

Even if the (001) surface is the most stable, the {001} planes are not the most exposed, because the hexagonal symmetry of HA generates six {010} faces which, hence, become the predominant faces in the habit. This is coherent with what experimentally observed.(ref) The (101) surface is present in the habit, hence it is not negligible, but it is less important as its exposed area is smaller than the two previous surfaces. Conversely, the Wulff construction highlights the disappearing of the (110) surface from the crystalline habit, because of a too large surface energy. Hence, we neglected the (110) surface in the treatment of water adsorption processes. Even if the surface energy of the stoichiometric (010) surface suggests a low importance, we decided not to ignore it, in order to obtain a full comparison between the three (010) terminations.

Interaction of the HA surfaces with water

In this second paragraph, the quantum-mechanical study of water adsorption upon the (001), (010) and (101) surfaces is discussed, in order to characterize exhaustively the behaviors of the most reactive sites, already identified by the electrostatic analysis (*vide supra*). As a matter of fact, the oxygen atom of the water molecule displays a negative potential, highlighted by a Mulliken net charge of -0.6 *e*, counterbalanced by the hydrogen atoms, each with a charge of +0.3 *e*. Following the electrostatic complementarity principle, already adopted by some of us in previous papers,(ref) we adsorbed water allowing the interaction of the oxygen atoms with the most exposed calcium ions. Consequently, the hydrogen atoms are free to establish H-bonds, either with the phosphate ions or with the hydroxyl ions or with other previously adsorbed water molecules. Indeed, we studied the increasing loading up to a coverage of more than 1.5 water molecules *per* exposed calcium ion upon each surface, i.e. a loading which brings to an almost complete coverage of the surface. In these conditions, it is highly probable that the adsorbed water molecules create a network of hydrogen bonds also among them and not only towards the reactive sites of the surface. This hypothesis has then been confirmed by the quantum-mechanical calculations: for instance, the top view of the (001) surface is reported as function of the loading (Figure 4). In the supplementary material, the loading for each surface is reported (Figures 1S, 2S, 3S and 4S). The coverage for the maximum loading case shields almost completely the HA surface.

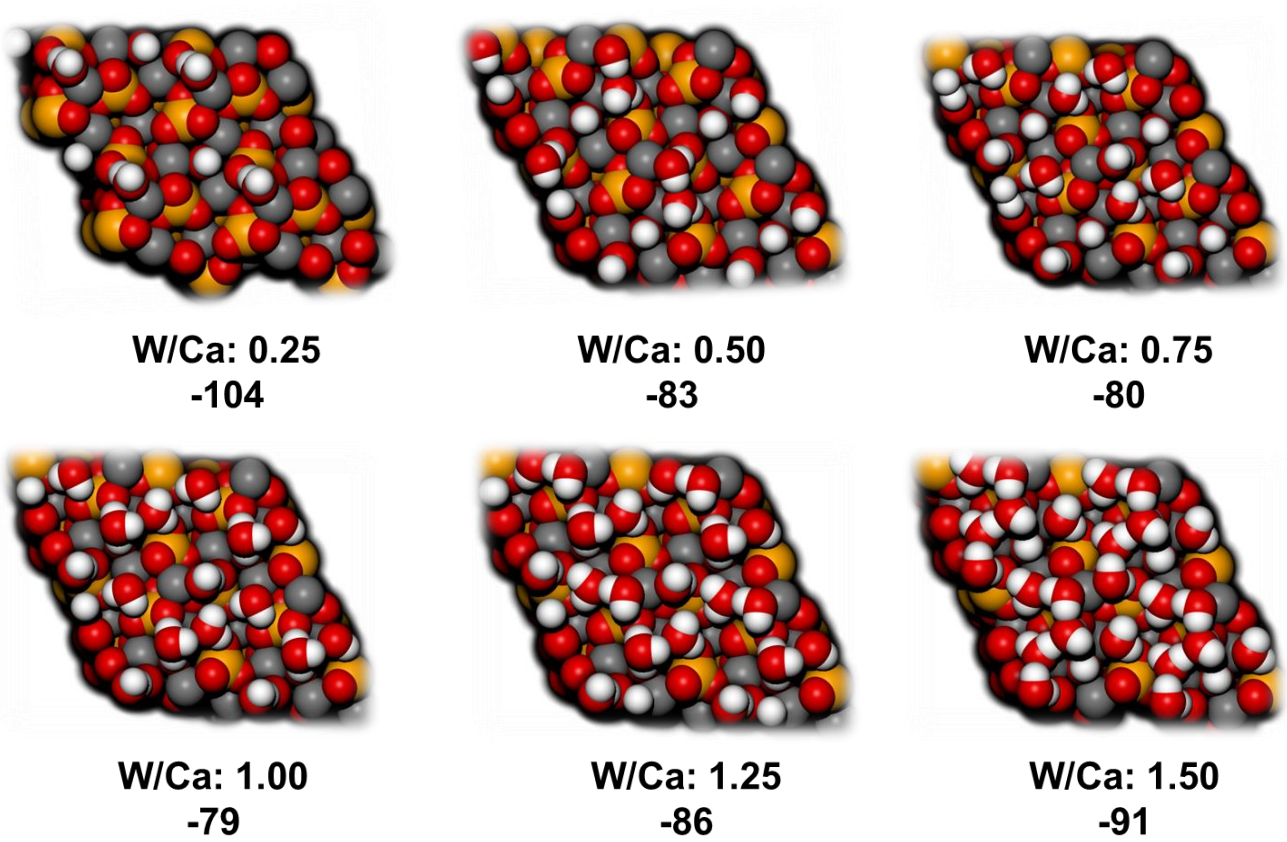

Figure 4. Top views of the increasing water loading for the (001) surface: W/Ca is defined as the number of water molecules *per* unit of exposed calcium ion and corresponding ΔH is expressed in kJ mol^{-1}. Color-coding: oxygen in red, hydrogen in white, calcium in gray and phosphorus in orange.

Physisorption or chemisorption?

From previous studies, it is well known that water can not only adsorb maintaining its molecular nature (*physisorption*), but can also dissociate, generating new CaOH and POH surface functionalities, if the adsorbing surface sites are particularly polarizing (*chemisorption*).(ref) In our case, water dissociation happens in only two cases: i) one water molecule dissociates upon the (010) stoichiometric surface and ii) two water molecules dissociate upon the (101) surface. The electronic reaction energies (BSSE-corrected and including the dispersive contribution) *per* water molecule are -245 kJ·mol^{-1} and -150 kJ·mol^{-1}, respectively. These very large energies strongly characterize the chemisorption processes, in which the molecular nature of the reactants is not preserved and chemical bonds are broken and new ones are created. Coherently, the (101) and the (010) stoichiometric slab structures were already identified to be the most reactive, because of their large surface energies. These water-reacted surfaces, hereafter (010) R and (101) RR, are considered as the substrate upon the which the physisorption process is studied, as these systems should more correctly represent the experimental terminations, being HA synthetized in a watery environment. This assumption has already been confirmed to reproduce more correctly the interaction between HA and other molecules.(ref) The presence of the new CaOH functionalities deriving from the dissociation processes decreases the total number of Ca ions available for the physisorption, as some Ca ions have already been covered. Thus, from 4 Ca ions of the bare surfaces (Table 1), the (010) R and the (101) RR surfaces elicit only 3 and 2 Ca ions, respectively.

Dissecting the physisorption energies

The energetics of the physisorption processes is reported in Table 2. It is noteworthy, first of all, that the use of the current basis set brings the BSSE to affect the BE for less than 15 % for every case. This is a very important improvement with respect to previous results in which the BSSE affected the BE for more than 40 %, because of a less rich basis set.(ref) The present results are, then, much more accurate and reliable.

Table 2. Computed energetic parameters describing the water physisorption processes at the studied HA surfaces, for different loading. Ca/S is the number of exposed Ca^{2+} ion *per* surface unit cell. θ is the loading ratio, i.e. the number of water molecules *per* number of exposed Ca^{2+}ions. All the energy parameters are in kJ·mol^{-1}.

HA	Ca/S	θ	ΔE_S	ΔE_M	ΔE_L	ΔE_L^C	ΔE^*	ΔE^{*C}	ΔE	ΔE^C	BSSE	ΔE^D	ΔH
(001)	4	0.25	24.1	9.4	-0.7	-0.7	-145.4	-135.2	-112.6	-102.4	-10.2	-9.5	-103.7
		0.5	18.4	6.6	-2.3	-1.1	-113.7	-101.9	-89.8	-78.0	-11.8	-14.3	-83.5
		0.75	18.6	4.6	-1.8	-0.5	-105.5	-92.9	-82.8	-70.2	-12.6	-17.1	-77.1
		1.0	13.9	3.1	-7.4	-5.6	-88.8	-76.9	-77.4	-65.4	-12.0	-17.3	-72.8
		1.25	15.1	2.6	-8.1	-5.4	-93.8	-81.9	81.6	-69.6	-12.0	-16.5	-75.8
		1.50	15.8	2.6	-10.5	-7.1	-93.4	-80.8	-82.1	-69.5	-12.6	-17.2	-76.0
(010) R	3	0.33	19.5	5.4	1.3	1.3	-137.3	-122.6	-111.2	-96.5	-14.7	-19.8	-107.5
		0.66	21.1	3.0	-9.2	-7.3	-118.8	-104.4	-101.9	-87.5	-14.4	-18.4	-95.1
		1.00	19.2	2.4	-4.0	-1.9	-115.2	-102.0	-95.6	-82.4	-13.2	-18.3	-90.1
		1.33	19.0	2.3	-4.0	-1.4	-107.4	-94.2	-87.6	-74.4	-13.2	-19.0	-82.6
		1.66	18.8	2.1	-8.9	-5.8	-95.6	-83.4	-80.5	-68.3	-12.3	-19.1	-76.6
(010) Ca-rich	3	0.33	11.3	1.9	-0.3	-0.3	-129.1	-115.5	-116.2	-102.6	-13.6	-17.2	-108.4
		0.66	13.5	3.4	-13.4	-11.9	-122.2	-112.4	-118.6	-107.4	-11.2	-13.9	-111.1
		1.00	35.3	3.5	-1.4	0.4	-151.9	-139.8	-114.5	-100.6	-13.8	-15.7	-105.8
		1.33	35.0	2.5	6.8	9.2	-151.1	-138.3	-106.9	-91.6	-15.2	-18.5	-99.4
		1.66	30.6	1.9	5.5	8.9	-135.6	-123.4	-97.6	-81.9	-15.7	-18.9	-90.0
(010) P-rich	3	0.33	34.9	3.4	-0.2	-0.2	-188.4	-173.6	-150.2	-135.4	-14.8	-22.0	-146.4
		0.66	26.3	2.8	2.2	2.8	-150.8	-142.6	-118.9	-110.7	-8.2	-16.9	-117.1
		1.00	22.0	2.4	3.1	4.1	-133.5	-120.7	-105.0	-92.3	-12.7	-18.2	-100.0
		1.33	17.5	1.8	-4.8	-2.7	-111.4	-98.6	-94.8	-82.0	-12.8	-18.8	-90.0
		1.66	18.1	2.1	-11.3	-8.2	-104.2	-92.1	-92.3	-80.2	-12.1	-17.7	-87.0
(101) RR	2	0.50	30.7	3.0	-0.8	-0.8	-173.9	-159.2	-141.0	-126.3	-14.6	-22.2	-137.5
		1.00	33.6	2.0	3.1	4.2	-162.2	-147.7	-123.5	-109.0	-14.5	-19.3	-117.0
		1.50	45.6	4.0	5.4	6.4	-166.4	-152.9	-111.3	-97.9	-13.4	-16.0	-103.4

The dispersive forces contribution (BE^D), which depends on the geometry only, is nearly constant to an averaged value of 18 kJ·mol^{-1}. The very first water molecule adsorbed at the (001) surface presents a lower BE^D because it is interacting with the most exposed Ca^{2+} ion and, as the dispersive contribution depends only on the geometry (i.e. the more the atoms surrounding the molecule, the larger the dispersive term), the BE^D is justified to be low in this particular case.

In general, the molecular deformation (ΔE_M) is almost negligible (less than 10 kJ·mol^{-1}) and decreases with the loading, meaning that the first interacting molecules are adsorbed upon the strongest sites of the surface, while the subsequent ones feel weaker sites which less deform the molecules.

Analyzing the trends of the surface deformation energies (ΔE_S) as functions of the increasing loading, two different behaviors can be highlighted. On the one hand, the deformation energies of the (001), the (010) R and the (010) P-rich surfaces decrease with the loading to a value between 15 and 20 kJ·mol^{-1}. This means that the first adsorbed molecules deform the surfaces more than the subsequent ones. On the other hand, the surface deformation energies of the (010) Ca-rich and the (101) RR surfaces increase with the loading, up to more than 30 kJ·mol^{-1}. A cooperative effect between the adsorbates is then highlighted which further deform the surface.

The lateral interactions between the adsorbates (ΔE_L^C, BSSE-corrected) show again two different trends. The (001), (010) R and (010) P-rich exhibit decreasing trends, towards negative values. This means that the adsorbed molecules prefer to rearrange and to establish a stabilizing pattern of hydrogen-bond interactions between them, rather than to establish new interaction with the HA ions. These attractive interactions partially compensate the surface and molecular deformation energies, leading the BE^{*C} values (the binding energies BSSE-corrected and free of the deformation

and lateral interaction terms) to be close to the correspondent BE^C values. Conversely, the (010) Ca-rich and (101) RR surfaces show positive lateral interaction values, which increase with the loading. Hence, the correspondent BE^{*C} values increase and diverge from BE^C, as the lateral interactions do not compensate the deformation energies. In order to understand the positive value of the lateral interactions, a deeper analysis was performed and is presented in the next sub-paragraph.

Electronic and geometric features of the adsorption

We calculated, as functions of the increasing loading: (i) the averaged Mulliken charges of the water molecules adsorbed upon the surfaces, (ii) the averaged Ca---O_W distance (between the exposed Ca^{2+} ions of the surface and the oxygen atoms of the water molecules) and (iii) the averaged H-bond length between the hydrogen atom of the water molecule and the acceptor oxygen atom.

The results are reported in Figure 5 (section A, B and C).

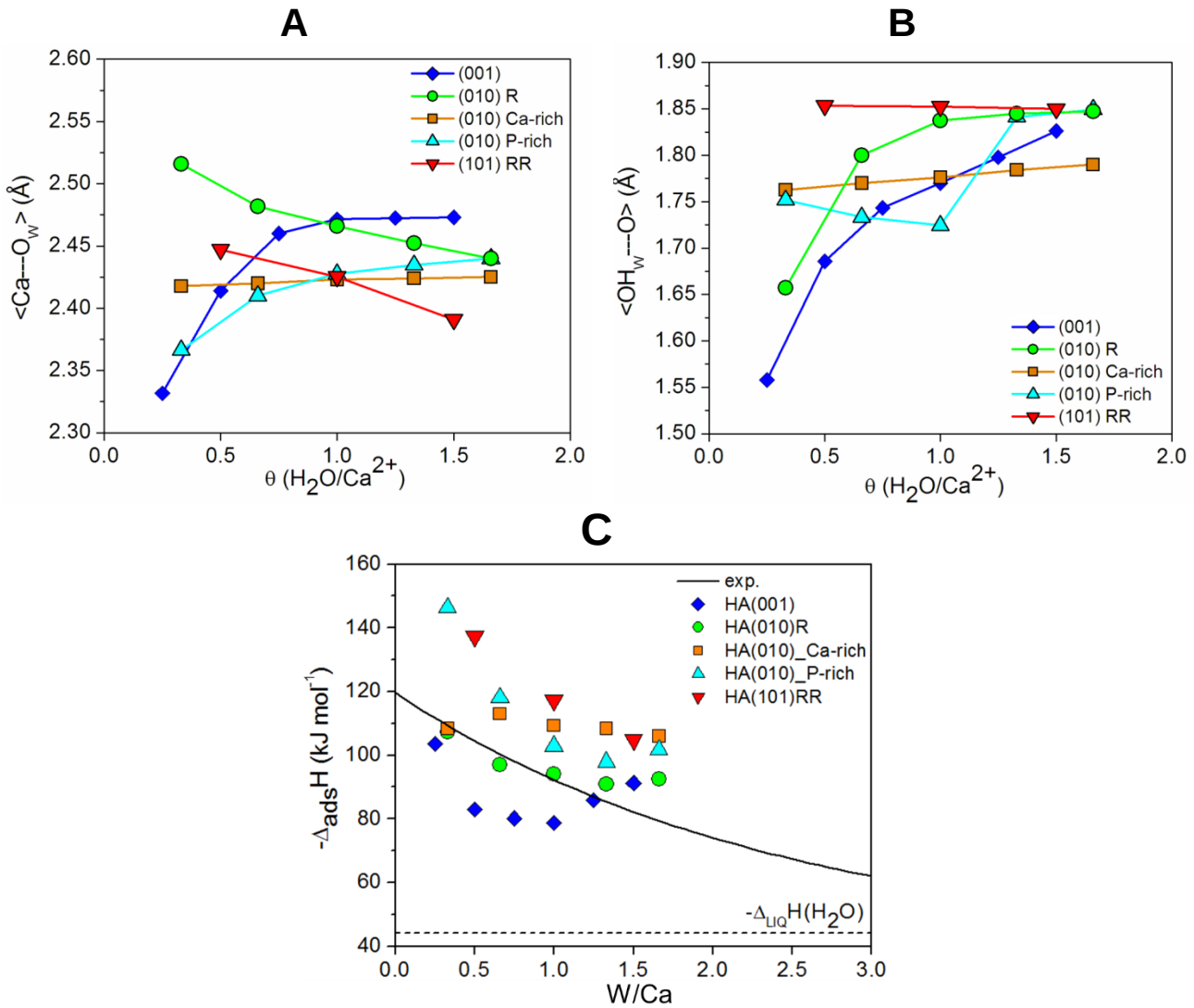

Figure 5. Variations of the averaged Ca---O_W (**A**) and OH_W---O (**B**) intermolecular bond lengths, as function of the loading ratio (number of water molecules *per* number of exposed calcium ions). Heat of adsorption for each surface, compared with the experimental trend (**C**).

For the (001), (010) R and (010) P-rich surfaces, the charge transfer from the surface to the water molecules decreases with the loading, as the value goes towards zero. The Ca---O distance and the H-bond length increase from very small values (2.3 Å and 1.5 Å, respectively) towards larger ones (2.5 Å and 1.85 Å, respectively). For the (010) P-rich surface, the H-bond length initially decreases (for the three lower cases), because of strong unsaturated phosphate ions which characterize the P-rich structure. Once they are saturated, the H-bonds lengthen towards a *plateau* value of 1.85 Å.

These data suggest that these surfaces are "classical": after covering the first attractive and strong sites of the surfaces, their adsorption affinity decreases and the subsequent water molecules prefer to interact among them rather than with the surface (long Ca---O_W distances, long H-bonds, low BE^{*C} values, low charge transfer and large lateral interactions). For instance, the (001) surface is characterized by one very exposed Ca^{2+} ion which leads the reactivity of this surface. Once this ion has been saturated with a molecule, the surface decreases its strength, as all the other Ca^{2+} ions are less exposed and, hence, less reactive.

Conversely, the (010) Ca-rich and (101) RR surfaces behave differently. The charge transfer increases as the averaged net Mulliken charge of the adsorbed water molecules assumes more negative values, going towards -0.03 e. The averaged Ca---O distances become shorter than the previous cases, aiming at 2.4 Å *circa*. The averaged H-bond length for these surfaces does not significantly vary with the loading and, for the (010) Ca-rich surface, it reaches the very lowest value (1.75 Å). The (101) RR surface presents, instead, long H-bonds (1.85 Å), because of the presence of two dissociated water molecules upon the surface. These molecules already saturate the most reactive phosphate ions and oblige the subsequent water molecules to establish long H-bonds. The BE^{*C} values are very large and increase with the loading, above all for the (010) Ca-rich surface.

These results highlight how the (010) Ca-rich and the (101) RR surfaces enhance their reactivity towards polar molecules with the increasing loading. The large surface deformation energy indicates that the ions of these surface become more exposed and, thus, more reactive when the loading increases. The positive lateral interaction are, then, due to the water molecules which prefer the direct interaction with the reactive surface sites, thus neglecting (or even contrasting) the establishment of H-bonds between the adsorbates. Anyway, the gain in BE^{*C} is large enough to provide the BE^{C} of these two surfaces comparable to those of the other.

Enthalpy of physisorption

From the BE^C and BE^D values, it is possible to calculate the enthalpy of adsorption, properly considering the thermal contributions (see section 2.2). The theoretical data are, then, compared to the experimental microcalorimetric trend of water adsorption at different nano-crystalline HA samples.(ref) The results are reported in Figure 5 (section C) and highlight a striking correspondence for the (010) surfaces. This is in agreement with the experimental crystalline habit of HA, in which the (010) surfaces are predominant.(ref Rimola/gly) Conversely, the (001) and the (101) surfaces do not reproduce very well the experimental behavior, confirming their less importance in the description of the habit.

Conclusions

In this paper we studied at a DFT/B3LYP level of theory, using the CRYSTAL code, the most important surfaces of the crystalline hexagonal hydroxyapatite ($Ca_{10}(PO_4)_6(OH)_2$). HA is one of the most investigated biomaterial, since it constitutes the majority of the mineral phase of bones and teeth. Its biocompatibility is successfully exploited in many biomedical applications, from prostheses to component of toothpastes. Hence, the study of its surfaces is very important when trying to understand the interactions between the material and the molecules. Here, after analyzing the most important surfaces of HA, we investigated their interactions with the ubiquitous molecule in biological fluids, water.

From a complete description of geometrical, electronic and energetic properties of the surfaces, we predicted the crystalline habit of HA through the Wulff constructions, also characterizing at a molecular level the terminations of the surfaces. We found that the most stable termination along the [010] direction is not the stoichiometric surface. Indeed, the non-stoichiometric surfaces, which depend on the chemical potential of calcium phosphate, are more stable than the stoichiometric surface at any value of chemical potential.

The adsorbed water molecules dissociated upon the two most reactive surfaces, i.e. the stoichiometric (010) and (101) surfaces. The physisorption process leaded upon the reacted substrates on these two surfaces and upon all the remaining surfaces revealed two kind of behaviors. A first set of surfaces decreases the reactivity with the loading of water molecules, meaning that this kind of surface decreases the affinity towards water, after covering the most reactive sites with the first molecules. The second typology of surfaces behave oppositely, i.e. the increasing coverage of molecules enhances the reactivity of this substrate.

From the

Acknowledgements

The largest calculations presented in this research have been supported by generous allowance of computer time from CINECA computing center (Project ISCRA_SILDRUG). The CRYSTAL team headed by R. Dovesi (Dip. Chimica, University of Torino) is acknowledged for providing the development version of the CRYSTAL14 code.

F. References

1. Chiatti F, Corno M, Ugliengo P (2012) Stability of the Dipolar (001) Surface of Hydroxyapatite. J Phys Chem C 116:6108–6114.

2. Astala R, Stott MJ (2008) First-principles study of hydroxyapatite surfaces and water adsorption. Phys Rev B 78:75427.

3. Dovesi R, Orlando R, Erba A, et al. (2014) CRYSTAL14 : A program for the ab initio investigation of crystalline solids. Int J Quantum Chem 114:1287–1317.

4. Kohn W, Sham LJ (1965) Self-consistent equations including exchange and correlation effects. Phys Rev 140:A1133–A1138.

5. Hohenberg P, Kohn W (1964) Inhomogeneous electron gas. Phys Rev 136:B864–B871.

6. Ugliengo P, Viterbo D, Chiari G (1993) MOLDRAW: Molecular Graphics on a Personal Computer. Z Krist 207:9–23.

7. Tarini M, Cignoni P, Montani C (2006) Ambient occlusion and edge cueing to enhance real time molecular visualization. IEEE Trans Vis Comput Graph 12:1237–1244.

8. Humphrey W, Dalke A, Schulten K (1996) VMD: Visual Molecular Dynamics. J Mol Graph 14:27–28,33–38.

9. Schäfer A, Horn H, Ahlrichs R (1992) Fully Optimized Contracted Gaussian Basis Sets for Atoms: Li to Kr. J Chem Phys 97:2571.

10. Becke AD (1993) Density-functional thermochemistry. III. The role of exact exchange. J Chem Phys 98:5648–5652.

11. Lee C, Yang W, Parr RG (1988) Development of the Colle-Salvetti correlation-energy formula into a functional of the electron density. Phys Rev B 37:785–789.

12. Corno M, Chiatti F, Pedone A, Ugliengo P (2011) In silico study of Hydroxyapatite and Bioglass®: how computational science sheds light on biomaterials. Biomater. / B. 1

13. Corà F, Alfredsson M, Mallia G, et al. (2004) The performance of hybrid density functionals in solid state chemistry. Struct Bond 113:171–232.

14. Corno M, Busco C, Bolis V, et al. (2009) Water Adsorption on the Stoichiometric (001) and (010) Surfaces of Hydroxyapatite: A Periodic B3LYP Study. Langmuir 25:2188–2198.

15. Corno M, Orlando R, Civalleri B, Ugliengo P (2007) Periodic B3LYP study of hydroxyapatite (001) surface modelled by thin layer slabs. Eur J Min 19:757–767.

16. Monkhorst HJ, Pack JD (1976) Special Points for Brillouin-Zone Integration. Phys Rev B 8:5188–5192.

17. Dovesi R, Saunders VR, Roetti C, et al. (2014) CRYSTAL14, User's Manual. Università di Torino, Torino, Italy

18. Fletcher R (1970) A new approach to variable metric algorithms. Comput J 13:317–322.

19. Shanno DF, Kettler PC (1970) Optimal Conditioning of Quasi-Newton Methods. Math Comput 24:657–664.

20. Boys SF, Bernardi F (1970) The calculation of small molecular interactions by the differences of separate total energies. Some procedures with reduced errors. Mol Phys 19:553–566.